Flexible but robust $Ti_3C_2T_x$ MXene/bamboo microfibril composite paper for high-performance wearable electronics[†]

ⓘ Author and affiliation details can be edited in the panel that appears to the right when you click on the author list.

Wei-Bin Zhu[a], Feng-Lian Yi[a], Pei Huang[a,b,*], Hao Zhang,(ⓘD 0000-0003-0541-5830)[a], Zhen-Hua Tang[a], Ya-Qin Fu[c], ~~YouYong~~ You-Yong Wang[a], Jun Huang[a], Guang-He Dong[a], Yuan-Qing Li,(ⓘD 0000-0002-0478-0177)[a,b,*] and Shao-Yun Fu[a,b,*]

[a]College of Aerospace Engineering, Chongqing University, Chongqing 400044, China, p.huang@cqu.edu.cn, yqli@cqu.edu.cn, syfu@cqu.edu.cn

[b]State Key Laboratory of Power Transmission Equipment & System Security and New Technology, Chongqing University, Chongqing 400044, China

[c]Key Laboratory of Advanced Textile Materials and Manufacturing Technology of Ministry of Education, Zhejiang Sci-Tech University, Hangzhou 310018, China
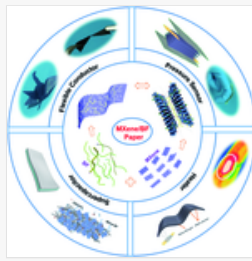
Funding Information

Table of Contents Entry

This work reports a flexible yet robust $Ti_3C_2T_x$ MXene/bamboo microfibril (BF) composite paper *via* a simple vacuum filtration process.

Abstract

This work reports a flexible yet robust $Ti_3C_2T_x$ MXene/bamboo microfibril (BF) composite paper *via* a simple vacuum filtration process. Due to the excellent compatibility between MXene and BF, the MXene/BF composite paper demonstrates simultaneously an excellent tensile strength of 49.5 MPa, higher than that of both MXene sheet and BF film alone and also among the top values compared with those in the literature, an excellent electrical conductivity as high as 4.8×10^3 S m^{-1} which is also higher even at a lower MXene content than those reported in the literature, and outstanding electrical stability with no detectable deterioration after 1000 cycles of stretching, bending and compression. As a result, the MXene/BF composite paper shows versatility for making various high-performance wearable electronics. Specifically, the as-prepared flexible pressure sensor by stacking exhibits a high sensitivity of 0.153 kPa^{-1} and a linear sensing performance in the pressure range of 0 to 2.5 kPa; the as-fabricated electric heater displays outstanding electrothermal performance, giving a temperature difference of 20 °C in air at the lowest input voltage of 2.5 V compared with those of the literature; the produced wearable symmetric all-solid-state supercapacitor achieves large enhancements in volumetric capacitance and gravimetric capacitance compared with the neat MXene supercapacitor and outstanding energy storage stability upon varied deformations. The MXene/BF composite paper with the above virtues is appealing for wide applications in multifunctional wearable electronics.

Introduction

In the past few decades, wearable devices have been developing rapidly.[1–5] The key to fabricate wearable devices lies in the acquirement of appropriate flexible conductors, which are mainly produced by the introduction of conducting materials into flexible matrices.[6–8] For example, a wrinkled graphene based conductor exhibited good stretchability and room-temperature self-healing, and was used as a strain sensor to monitor stretching deformation and human motion;[9] a carbon nanotube/polyurethane composite conductor was designed for preparing ultrastretchable strain sensors;[10] a kirigami silver nanowire/polyimide conductor was made for personal thermal management and motion detection.[11] In the meantime, the increased needs with regard to multifunctionality require wearable conductors not only to be highly conductive, mechanically robust and flexible, but also to have additional attributes such as stable mechanical, electrical and electrochemical properties under deformation, *etc.*,[12–15] whereas most of the flexible conductors reported hardly satisfy these demands. Thus, it is highly desirable to develop wearable conductors with the above-mentioned attributes for high-performance flexible electronics.

$Ti_3C_2T_x$ as one of the most intensively researched MXenes is generated by selectively chemical-etching out the Al element layers from the metallic layer Ti_3AlC_2 phase precursor.[7] Characterized by the exceptional electrical conductivity (6.5×10^5 S m^{-1}), easy production, large aspect ratio, fast ion diffusion rate and high volumetric capacitance, MXene sheets have been identified as an ideal candidate for wearable conductor materials.[16–18] However, the MXene films generally exhibit poor mechanical strength, limited flexibility and electrochemical properties because of the weak interlayer bonding between rigid MXene blocks, thus hindering their applications as flexible wearable electronics.[19–21] To overcome this shortcoming, various types of polymers have been applied to improve the interlayer bonding of MXene sheets at the cost of electrical conductivity and electrochemical properties due to the formation of an insulating layer between MXene sheets. For instance, the introduction of poly(vinyl alcohol) increased the tensile strength of MXene film from 22 MPa to 43 MPa, but led to a poor conductivity of 1.3 S m^{-1} (reduced from 240 238 S m^{-1}).[22] The addition of polydimethylsiloxane elastomer provided MXene film with desired flexibility and high

tolerance to stretching, bending and twisting, but inevitably led to a very low electrical conductivity of 0.63 S m^{-1}.[23] Although the incorporation of conductive polymers into MXene film retained its electrical conductivity, it brought about very poor tensile strength and limited electrochemical properties.[24–26] It appears that the combination of MXene with polymers cannot make flexible conductors with simultaneously high conductivity, high mechanical strength and high flexibility, as well as stable mechanical, electrical and electrochemical properties under various deformations.[27,28]

Bamboo microfibrils (BFs), ~~featuring~~featured by abundance, high aspect ratio, biocompatibility, excellent mechanical strength and flexibility, have been widely used as reinforcing blocks to construct functional composites.[29–34] It is worth noting that, compared with polymers in improving the mechanical performance of fragile MXene, hydrophilic ~~bamboo fibers~~BFs bear striking resemblance to delaminated MXene nanosheets with plenty of hydroxyl groups, which is beneficial for interfacial combination with functional groups of MXene in covalent-bond reactions or hydrogen-bond interactions.[35–37] This would likely promote the stress transfer between BFs and MXene, as significant improvements in tensile strength, flexural strength and hardness have been found in BF/graphene composites.[38] More importantly, the large aspect ratio of BFs would not only restrain the stacking of MXene nanosheets, but also avoid the non-linkage of MXene nanosheets, which might be expected to improve the mechanical strength and flexibility of MXene and also promote the electron transfer between MXene sheets.[39–41] The combination of MXene with BFs as conductors is expected to afford flexible electronics with the above-mentioned attributes but it has not been reported yet.

Owing to the excellent compatibility between MXene and BFs, high-performance $Ti_3C_2T_x$ MXene/BF composite paper is first produced by a simple vacuum filtration process. The combination of robust BFs and conductive MXene nanosheets produces the flexible but robust MXene/BF composite paper with high mechanical strength, good flexibility and excellent electrical conductivity. Moreover, the electrical conductivity of MXene/BF paper is highly stable upon 1000 cycles of deformations under stretching, bending and compression. Furthermore, the MXene/BF composite paper is demonstrated to be highly versatile in manufacturing wearable electronics such as pressure sensors, electric heaters and supercapacitors. Considering its extraordinary mechanical and electrical performances, easy processing and environmental friendliness, the MXene/BF composite paper is highly attractive for developing multipurpose wearable electronics.

Experimental section

Materials

Ti_3AlC_2 powders (98.0%; 400 mesh) were purchased from Jilin 11 Technology Co., Ltd. Hydrochloric acid (HCl, 36.5%), lithium fluoride (LiF, AR), sodium sulfate, anhydrous ethanol, sodium hydroxide, sodium hypochlorite, acetic acid, acrylamide (AAm), N,N-methylenebisacrylamide (MBAA), ammonium persulfate (APS), sodium hyaluronate (SH) and N,N,N',N'-tetramethylethylenediamine (TEMED) were obtained from Chuandong Chemical Ltd (China). Polydimethylsiloxane (PDMS, SYLGARD 184) was provided by Dow Corning Inc. All the materials were used without further purification. Bamboo microfibrils were prepared as reported previously.[42] Typically, chopped mesh bamboo was soaked in sodium hydroxide solution (3.5 M) at 180 °C for 12 h in a Teflon-lined stainless steel reactor. Following neutralization with sodium hypochlorite solution (2.5 M) and rinsing with deionized water, the bamboo microfibrils were obtained after freeze–drying.

Synthesis of MXene sheets

$Ti_3C_2T_x$ (MXene) nanosheets were prepared as follows. Firstly, 0.5 g LiF powder and 0.5 g MXene precursor (Ti_3AlC_2) powder were consecutively added into 10 mL HCl solution (9 M). After continuous stirring at 35 °C for 24 h, the suspension was washed with water by centrifuging at 5000 rpm until pH > 6. Then, the precipitates were collected and sonicated for 1 h. Finally, the supernatant obtained by centrifuging at 3500 rpm for 1 h was freeze–dried, yielding the MXene powder.

Fabrication of MXene/BF composite paper

0.5 g MXene was dispersed in 250 mL deionized water under bath sonication for 1 h, and then mixed with BF suspension (0.5 wt%). Following 10 min sonication and 6 h mechanical stirring, the homogeneous suspension

produced was vacuum filtered and dried at 40 °C, yielding the MXene/BF composite paper. For the purpose of comparison, the pure BF paper and pure MXene paper were made in a similar way.

Fabrication of the wearable pressure sensor

The wearable pressure sensor was obtained by stacking 2, 4 or 6 layers of the MXene/BF composite paper with the dimensions of 20×10 mm^2. Both the bottom and top layers were attached with foil electrodes, followed by PDMS encapsulation.

Fabrication of the wearable electric heater

The MXene/BF composite heater was prepared by the encapsulation of the MXene/BF composite paper within PDMS films after the attachment of foil electrodes.

Fabrication of the flexible all-solid-state symmetric supercapacitor

The all-solid-state symmetric supercapacitor sealed by PDMS consists of the MXene/BF composite paper electrode and polyacrylamide (PAAm) hydrogel electrolyte. The MXene/BF electrode was produced by cutting the MXene/BF composite paper into dimensions of 20×5 mm^2 and then drop-casting with sodium sulfate solution. The PAAm hydrogel electrolyte was produced by mixing the PAAm hydrogel with sodium sulfate solution and 0.25 wt% TEMED at 45 °C for 1 h; the PAAm hydrogel was synthesized by introducing MBAA (0.06 wt%) as the crosslinker and APS (0.16 wt%) as the initiator into the AAm aqueous solution (2.17 M) at 45 °C for 1 h.

Characterization

The microstructures of BFs, Ti$_3$AlC$_2$, MXene and MXene/BF composite paper were characterized using a scanning electron microscope (SEM, Phenom XL) equipped with an energy-dispersive X-ray spectroscope. The atomic force microscopy (AFM) and transmission electron microscopy (TEM) profiles were obtained using a Bruker scanning probe microscope (Dimension icon) and FEI Talos F200S G2 microscope, respectively. Fourier transform infrared (FTIR) spectra were obtained with a Thermo Nicolet NEXUS 670 FTIR *via* ATR mode. X-ray diffraction (XRD) patterns of BFs, Ti$_3$AlC$_2$, MXene and composite paper were recorded using a BRUKER D2 PHASER X-ray diffractometer (BRUKER AXS Co., Germany). The X-ray photoelectron spectroscopy (XPS) of BFs, MXene and composite paper was performed with a LabRAM HR Evolution and Thermo ESCALAB 250XI. All the optical images were taken using a digital camera (Canon 5D). The electrical conductivity of MXene/BF composite papers was measured with a resistance scanner (TH2518 and VICTOR 86E) through the two-probe method. The mechanical performance of the MXene/BF composite paper was investigated by using a universal testing machine (SHIMADZU AGS-X) at a displacement rate of 1 mm min^{-1}. To characterize the sensing performance of the MXene/BF based pressure sensor, the electrodes of the sensor were connected to a digital multimeter (KEYSIGHT 34465A). The relative change of the resistance (RCR) is defined as RCR $= |R_s - R_0|/R_0$, where R_0 and R_s are the resistance without and with the applied pressure. The thermal images of the MXene/BF heater were taken using an infrared camera (FLIR E6). All the electrochemical measurements of the supercapacitor were performed in a typical two-electrode cell using an electrochemical workstation (CHI600E). Cyclic voltammetry (CV) tests at different scan rates (1, 5, 10, 20, 50, 100, and 200 mV s^{-1}) from 0 to 0.7 V, and galvanostatic charge–discharge (GCD) at various current densities from 0 to 0.7 V were carried out. The cycling stability test of the as-prepared supercapacitor was conducted at room temperature for 1000 loops. The capacitance (C) is calculated through the following equation:

$$C = \frac{1}{2Uv} \int_{U^-}^{U^+} I \mathrm{d}U \tag{1}$$

where I, U and v are the current density, potential window and potential scan rate, respectively. The gravimetric (C_g) and volumetric specific capacitance (C_V) are calculated from eqn (2) and (3), respectively.

$$C_g = \frac{C}{m} \tag{2}$$

$$C_v = \frac{C}{V}$$

where m and V are the mass and volume of the active materials in electrodes, respectively.

Results and discussion

Fabrication and characterization

MXene/BF paper was self-assembled by the vacuum filtration of MXene and BF suspension (Fig. 1a). The MXene sheets, produced by selective etching of Ti_3AlC_2 (Fig. S1a and b[†]), preserve a symmetric hexagonal structure and high crystallinity (Fig. 1b), and have a uniform thickness of 4.3 nm and a lateral size of 2–3 μm (Fig. 1c).[43,44] XRD patterns from Ti_3AlC_2 to MXene reveal that the characteristic diffraction peak (002) shifts from 9.45° to a smaller angle (7.35°) and most peaks of Ti_3AlC_2 disappear in the MXene pattern, indicating the increase of interlayer space and removal of the Al layer in Ti_3AlC_2 by the etching process (Fig. 1d). Additionally, the XRD patterns of MXene and MXene/BF paper show that the characteristic diffraction peak (002) of MXene shifts to a smaller angle (6.55°) with introduction of MXene into BFs, indicating that the interlayer spacing is enlarged from 1.203 nm to 1.349 nm. The bamboo microfibrils have a diameter of 2–30 μm and a length of several millimeters (Fig. S1c[†]). Due to the abundant oxygen-related groups (Fig. 1e), a red-shift of 3434 cm^{-1} in MXene and 3427 cm^{-1} in BFs to 3430 cm^{-1} is observed in the MXene/BF composite paper (Fig. 1f), indicating the formation of hydrogen bonding between MXene sheets and BFs. The excellent compatibility between MXene sheets and BFs was also supported by the firm coating of MXene sheet onto BFs in the freeze–dried sample (Fig. S1d[†]). As shown in Fig. 1g and h, the MXene film preserves a wrinkled surface while the BF paper possesses a rough surface with partially visible bamboo fibers because of the aggregation of big fiber bundles. Due to the good interfacial adhesion between MXene sheets and BFs, the MXene/BF composite paper exhibits a homogeneous wrinkled surface similar to that of MXene paper (Fig. 1i), evidenced by the uniform distribution of Ti, F, C and O in the MXene/BF paper (Fig. S1e[†]). Moreover, as shown in Fig. S2a–c,[†] the fracture cross-section of the neat MXene film exhibits a densely packed layered structure after the removal of Al element, while the pure BF film exhibits a similar layered structure, but has vast interlayer gaps and discontinuities. In comparison, the MXene/BF film shows a loosely layered structure combined with interlayer spacing and gaps, which is similar to nacre's brick-mortar structure.[45,46] The layered structure of the MXene/BF composite paper provides vast gaps in the case of MXene aggregation, favorable for the electron transfer between MXene sheets. Moreover, the MXene/BF composite paper possessed a large specific surface area because of the wrinkled and loose nacre-like structure, endowing the composite paper with improved mechanical and electrical properties, and potential functionalization reliability.

Fig. 1
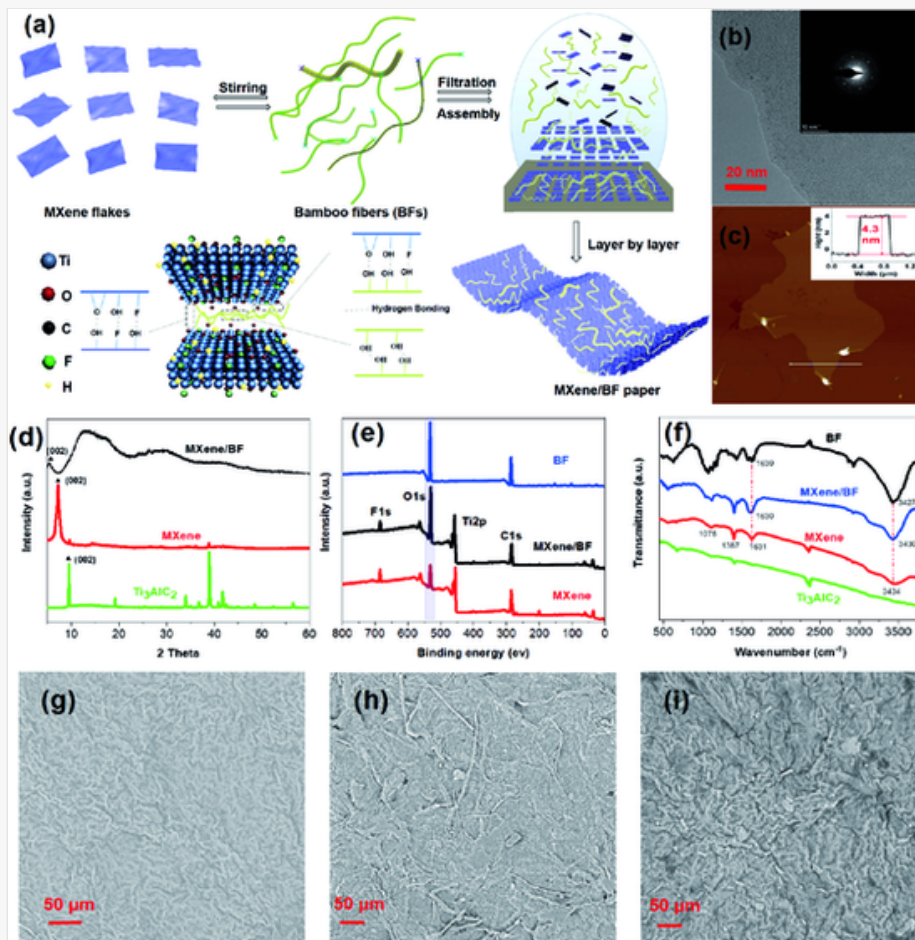
(a) Schematics for the preparation of the MXene/BF composite paper. (b) TEM image of the MXene sheet. The inset represents the selected-area electron diffraction (SAED) pattern. (c) AFM image of the MXene nanosheet on mica. The inset is the line profile for the MXene sheet marked by a white line in the image. (d) XRD patterns of Ti_3AlC_2, pure MXene and MXene/BF paper. (e) XPS survey spectra of BFs, MXene, and MXene/BF (50 wt%, 60 μm in thickness) composite paper. (f) FTIR spectra of Ti_3AlC_2, pure BFs, pure MXene, and MXene/BF (50 wt%, 60 μm in thickness) composite paper. (g–i) SEM images of neat MXene (g), neat BFs (h) and MXene/BF (50 wt%, 60 μm in thickness) composite paper (i).

As shown in Fig. 2a and b, the pure MXene paper exhibits a poor tensile strength of 5.26 ± 1.25 MPa, a low toughness of 0.14 ± 0.05 MJ m^{-3}, and an elongation at break of 2.64 ± 0.55%, in agreement with the previous report.[47] After

the introduction of BFs, the mechanical properties are greatly enhanced. It is worth noting that the mechanical properties of the MXene/BF film with more than 50% BFs are superior to those of the pure BF film. To be specific, the BF film has a tensile strength of 34.77 ± 2.25 MPa, a toughness of 0.88 ± 0.10 MJ m^{-3}, and an elongation at break of $4.03 \pm 0.50\%$ while the MXene/BF paper of 50 wt% BFs possesses a tensile strength of 49.46 ± 2.25 MPa, a toughness of 1.65 ± 0.30 MJ m^{-3} and an elongation at break of $6.12 \pm 0.55\%$, and even can withstand a weight of 20 g (Fig. S3[†]). The considerable improvement in the mechanical performance is due to the fact that the excellent compatibility between BFs and MXene benefits the stress transfer from BFs to MXene.[45,48]


Fig. 2
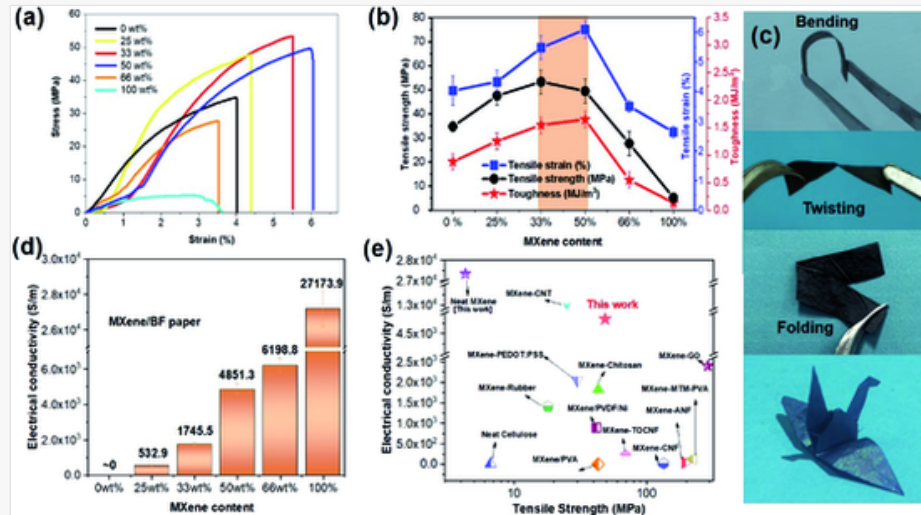
(a) Tensile stress–strain curves and (b) tensile strength, strain and toughness of the MXene/BF composite papers with various MXene contents; (c) excellent flexibility indication of the composite paper with a 50 wt% MXene content under bending, twisting and folding; the paper crane made of the MXene/BF paper shows the excellent flexibility; (d) electrical conductivity of the MXene/BF composite papers; and (e) comparison of the electrical conductivity and tensile strength of the MXene/BF composite paper (50 wt%, 60 μm in thickness) with other MXene-related materials.[19,22,25,51–59]

In addition to the enhanced mechanical strength, the MXene/BF composite paper is highly flexible to fabricate a paper crane, and no visible damage is observed after severe bending, twisting and folding as shown in Fig. 2c. More importantly, the MXene/BF composite paper preserves ultrahigh electrical conductivity, which is favorable for the fabrication of a conductor and an electric switch (Movies S1 and S2[†]). As shown in Fig. 2d, high conductivity is achieved for the MXene/BF composite paper with 50 wt% and 66 wt% BFs, much higher than most of the MXene-based composites reported previously with even higher MXene contents (Table S1[†]).[17,22,25,49–51] Compared with other MXene-based composites, the current MXene/BF composite exhibits superior mechanical properties and electrical conductivity (Fig. 2e).[19,22,25,51–59] To strike a balance between mechanical performance and electrical conductivity, the MXene/BF paper with 50 wt% BFs was used as the model composition for further study.

Mechanical and electrical properties

As shown in Fig. 3a–c, the electrical resistance of the MXene/BF paper is nearly constant during stretching from 0 to 48 MPa, compression from 0 to 5000 kPa and bending from 0 to 180°. In addition, no detectable deterioration in electrical stability is seen after long-term stretching, bending and compression, suggesting the high reliability of the MXene/BF composite (Fig. 3d–f). To explore the high electrical stability over deformation, we characterized the microstructure of the MXene/BF composite at various states. As shown in Fig. 3g, the surface of the MXene/BF composite is covered with wrinkles derived from the folded MXene sheets at the initial state. After a tensile strain is applied, the number of wrinkles decreases, and the surface of the composite becomes much smoother, attributed to the flattening of MXene sheets (Fig. 3h). Owing to the high toughness and flexibility of BFs, the MXene/BF composite can withstand bending, stretching and compression without noticeable structural damage, and restore to its original state after the removal of external strain (Fig. 3i). This is to say, the conducting paths built by MXene sheets are well-preserved, bringing about high electrical stability.

Fig. 3
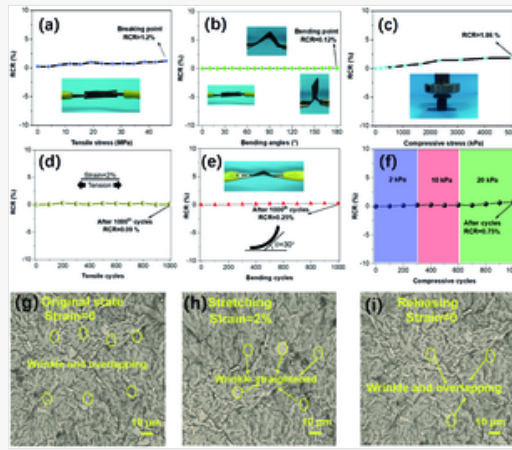
Electrical stability of the MXene/BF composite paper under various mechanical deformations. (a–c) RCR variation of the MXene/BF paper under (a) stretching, (b) bending from 0 to 1800 and (c) compression. (d–f) RCR variation of the MXene/BF paper over 1000 cycles by (d) stretching with the maximum strain of 2%, (e) bending and (f) compression under varied pressure. (g–i) SEM images of the MXene/BF film at initial (g), stretching (h) and releasing states (i).

In view of the high electrical stability and wrinkled surface, several layers of the MXene/BF composite paper were utilized to fabricate one flexible pressure sensor by stacking before encapsulation by PDMS films (Fig. 4a). As shown in Fig. 4b, a sensitivity of 0.071 kPa^{-1} is obtained for the two-layered MXene/BF pressure sensor. Significantly, the sensitivity of the pressure sensor can be manipulated by varying the layer number. When the layer number increases to 4 and 6, the sensitivity of the pressure sensor increases to 0.153 and 0.205 kPa^{-1}, respectively. Notably, the four-layered pressure sensor shows a linear sensing behavior in the pressure range of 0 to 2.5 kPa, which is comparable to other pressure sensors listed in Table S2.[†] Fig. 4c shows that peak RCR values of 20.5, 50.6 and 72.7% are achieved by the four-layered pressure sensor at the maximum pressures of 2, 5 and 20 kPa, respectively, agreeing with the results in Fig. 4b. In addition, the four-layered MXene/BF sensor shows a fast response time of 150 ms (Fig. 4d), suggesting potential for application in monitoring human movements, such as finger motion and air flow (Fig. 4e, f and Movie S3[†]).[60–62] The sensor is under tension and compression during finger bending as shown in Fig. 4e. Considering that the electrical resistance of the MXene/BF composite paper is nearly constant during stretching as shown in Fig. 3a, only the compression was measured using the MXene/BF composite sensor. Moreover, since little change occurs in the resistance of the monolayer MXene/BF composite paper upon compression in Fig. 3c, the pressure sensing of the sensor consisting of several layers of the composite paper is mainly dependent on the contact resistance between composite paper layers because of their wrinkled surfaces. The contact area ~~increases~~ varies ~~and then decreases~~ upon applying and removing compressive stress, thus resulting in the alternation of electrical resistance (Fig. 4g).[63–65] In the original state, the conductive paths are connected with partial continuities. Under compression, the inter-layer conductive networks would increase rapidly and the resistance of the sensor would be reduced under compression. As a result, under cyclic compressive loading, the resistance variance would show a cyclic behaviour feature as shown in Fig. 4c and d.

Fig. 4
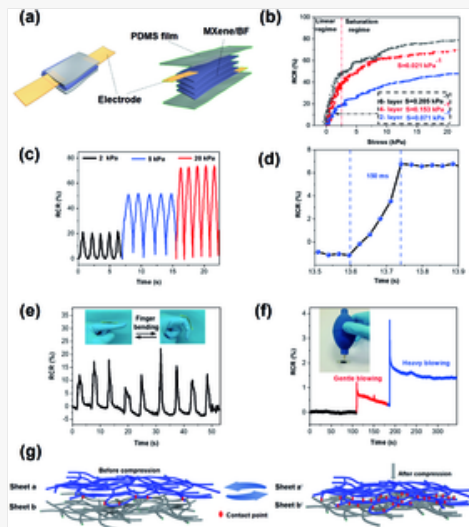
Sensing performance of the MXene/BF pressure sensor. (a) Schematic illustration of the MXene/BF pressure sensor. (b) RCR response of the MXene/BF pressure sensor with varied number of MXene/BF layers to pressure; *S* represents sensitivity. (c) RCR response of the MXene/BF pressure sensor under cycling pressure. (d) Response time of the MXene/BF pressure sensor under pressure. (e) RCR response of the pressure sensor with finger bending. (f) RCR response of the MXene/BF pressure sensor to airflow induced by a blowing gas pipe. (g) Schematics of the representative two-layer unit of the MXene/BF paper.

Wearable electric heaters are highly popular in thermotherapy as they can relieve pain and muscular stiffness by inducing vasodilation and increasing blood flow around the joints.[66] Owing to the superior conductivity as well as electrical stability over external stress, the MXene/BF composite paper was used to fabricate a wearable electric heater by encapsulation within PDMS (Fig. 5a). As shown in Fig. 5b, the temperature of the MXene/BF heater sharply increases within 2 minutes, and reaches a plateau which suggests an equilibrium state between heat generation and dissipation.[67] The temperature of the MXene/BF composite electric heater can be varied by the choice of voltage. Temperatures of 33.2, 38.1, 49.0 and 65.3 °C are obtained at the voltage of 1, 2, 2.5 and 3 V, respectively, consistent with the infrared images in Fig. 5c. Since the appropriate temperature for thermotherapy is 38–50 °C,[68] a voltage of 2.5 V is sufficient for the current MXene/BF heater, which is much lower than those of flexible heaters reported previously (Fig. 5d).[69–75] More importantly, the heater is highly reliable as a maximum temperature of *ca.* 46 °C and a minimum temperature of *ca.* 30 °C are obtained when a cyclic voltage of 2.5 V applied. The thermotherapy performance of the MXene/BF heater was demonstrated by wearing it on the wrist of a testee. As shown in Fig. 5f, the temperature of the heater is around 45 °C, much higher than that of the surrounding skin when a voltage of 2.5 V is applied. In comparison with other wearable electric heaters reported, the MXene/BF composite paper heater presents relatively higher mechanical strength and the lowest driving voltage as shown in Table S3.†

Fig. 5
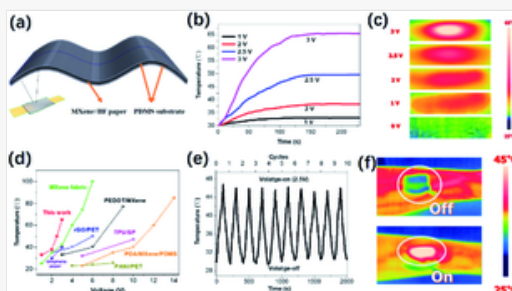
Electrothermal performance of the flexible MXene/BF heater. (a) Schematic illustration of the flexible MXene/BF heater. (b) Temperature–time curve of the flexible MXene/BF heater under varied working voltages. (c) Infrared camera images of the flexible MXene/BF heater under different voltages. (d) Comparison of the electrothermal performance of the MXene/BF heater with other heaters reported previously.[69–75] (e) Electrothermal response over cyclic voltage with a maximum value of 2.5 V. (f) Infrared images of the MXene/BF heater at on and off modes.

Apart from pressure sensing and thermotherapy, the MXene/BF composite conductor was further applied to produce a flexible all-solid-state symmetric supercapacitor. As shown in Fig. 6a, the flexible supercapacitor consists of MXene/BF paper electrodes, PAAm hydrogel electrolyte (Fig. S4†) and protective PDMS films. The CV curves of both MXene and MXene/BF supercapacitors maintain the rectangular-like shapes within the potential window (0–0.7 V) at different scan rates (1–200 mV s^{-1}) (Fig. 6b and S5a†). The specific volumetric capacitance of MXene and MXene/BF supercapacitors is around 0.81 F cm^{-3} and 2.23 F cm^{-3}, respectively, at the scan rate of 50 mV s^{-1} (Fig. S5b†). Moreover, the MXene/BF supercapacitor achieves a moderate specific gravimetric capacitance of 1.25 F g^{-1} at the scan rate of 50 mV s^{-1} (Fig. 6c), 5 times higher than that of the pure MXene supercapacitor. Additionally, the GCD curve gradually evolves from a distorted triangle to an isosceles triangle with the increase of current density (Fig. 6d). The capacity at low current density comprises pseudocapacitance caused by the oxidation–reduction process and ideal electrical double-layer capacitance, while the capacity at high current density is mainly derived from electrical double-layer capacitance. Notably, the MXene/BF supercapacitor shows a good long-term service, as 88.7% of the initial capacitance is retained after 1000 cyclic voltammetry scans at a scan rate of 100 mV s^{-1} (Fig. S5c†). The significant enhancement in energy storage is due to the fact that the introduction of BFs assists the dispersion of MXene sheets, and increases the electron-transfer pathway and active sites.[76–78] To our delight, the specific capacitance of the MXene/BF supercapacitor is well maintained at different bending angles as well as cyclic bending, twisting and folding, confirming the high stability of the MXene/BF supercapacitor (Fig. 6e and f). Supported by the above demonstrations, the excellent conductivity, mechanical strength and flexibility as well as significant electrical and electrochemical properties endow the MXene/BF paper with great potential in the fabrication of multipurpose wearable electronics, which is superior to those of other MXene-based devices as shown in Table S4.†

Fig. 6
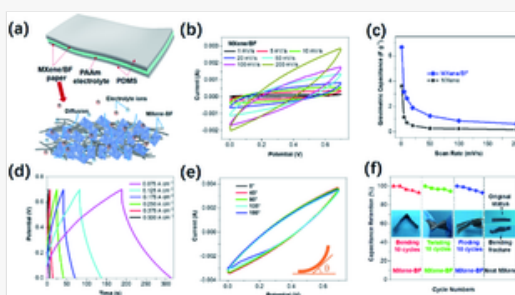
Electrochemical performance of the symmetric all-solid-state supercapacitors. (a) Schematic illustration of the MXene/BF all-solid-state supercapacitor and electrolyte ionic transportation through the layered structure. (b) Cyclic voltammetry (CV) curves of the device at the scan rate of 1–200 mV s^{-1}. (c) Calculated specific gravimetric capacitance of the MXene/BF composite supercapacitor and MXene supercapacitor at different scan rates. (d) GCD curves of the device at different current densities. (e) CV curves of the device at different bending angles. (f) Capacitance retention of the MXene/BF and MXene supercapacitors at cyclic deformations (the insets show the optical images of the supercapacitors at varied deformations).

Conclusions

A facile strategy has been proposed to fabricate a highly flexible yet robust conductor by the vacuum filtration of MXene sheets and BFs. The MXene/BF composite paper with 50 wt% BFs showed a tensile strength of 49.46 MPa and a conductivity of 4851.3 S m^{-1}, superior to most of the MXene-based materials. More importantly, the electrical conductivity of the MXene/BF composite paper is highly stable during bending, stretching and compression, hence making the MXene/BF composite an excellent conductor. Subsequently, the MXene/BF composite paper, by stacking, was employed to fabricate a pressure sensor, which has a sensitivity of 0.153 kPa^{-1} within the pressure range of 0–2.5 kPa. In addition, the MXene/BF-based wearable heater shows an excellent voltage-driven Joule heating performance. Owing to the much higher specific volumetric capacitance than pure MXene paper, the MXene/BF supercapacitor exhibits significantly improved storage capacity and stability over deformations. With such remarkable features, including high flexibility, high mechanical strength, superior stability and excellent conductivity over deformations, and enhanced specific capacitance, the current MXene/BF composite paper may enlighten the exploration of MXenes for various functional wearable electronics.

Author contributions

W. Z. was responsible for conceptualization, formal analysis, investigation, visualization, writing-original draft, and writing-review & editing. F. Y. was responsible for formal analysis, reviewing and editing. P. H. was responsible for conceptualization, formal analysis and investigation. H. Z. was responsible for software and conceptualization. Z. T. was responsible for formal analysis. Y. F. was responsible for investigation and resource. Y. W. was responsible for conceptualization. J. H. and G. D. were responsible for formal analysis and conceptualization. Y. L. and S. F. were responsible for visualization, resource, supervision and writing-review & editing.

Conflicts of interest

There are no conflicts to declare.

Acknowledgements

References

> (i) References can be edited in the panel that appears to the right when you click on a reference.

1 W. Zhang, P. Feng, J. Chen, Z. Sun and B. Zhao, *Prog. Polym. Sci.*, 2019, **88**, 220–240.

2 P. Huang, Y. Q. Li, X. G. Yu, W. B. Zhu, S. Y. Nie, H. Zhang, J. R. Liu, N. Hu and S. Y. Fu, *ACS Appl. Mater. Interfaces*, 2018, **10**, 11197–11203.

3 X. G. Yu, Y. Q. Li, W. B. Zhu, P. Huang, T. T. Wang, N. Hu and S. Y. Fu, *Nanoscale*, 2017, **9**, 6680–6685.

4 Z. Li, Z. Xu, Y. Liu, R. Wang and C. Gao, *Nat. Commun.*, 2016, **7**, 13684.

5 S. Luo, Y. A. Samad, V. Chan and K. Liao, *Matter*, 2019, **1**, 1148–1202.

6 P. Huang, Y. Li, G. Yang, Z.-X. Li, Y.-Q. Li, N. Hu, S.-Y. Fu and K. S. Novoselov, *Nano Mater. Sci.*, 2020, **3**, 1–16.

7 M. Naguib, V. N. Mochalin, M. W. Barsoum and Y. Gogotsi, *Adv. Mater.*, 2014, **26**, 992–1005.

8 L. Liang, Q. Li, X. Yan, Y. Feng, Y. Wang, H. B. Zhang, X. Zhou, C. Liu, C. Shen and X. Xie, *ACS Nano*, 2021, **15**, 6622–6632.

9 S. Yan, G. Zhang, H. Jiang, F. Li, L. Zhang, Y. Xia, Z. Wang, Y. Wu and H. Li, *ACS Appl. Mater. Interfaces*, 2019, **11**, 10736–10744.

10 Y. Gao, F. Guo, P. Cao, J. Liu, D. Li, J. Wu, N. Wang, Y. Su and Y. Zhao, *ACS Nano*, 2020, **14**, 3442–3450.

11 P. Won, J. J. Park, T. Lee, I. Ha and S. H. Ko, *Nano Lett.*, 2019, **19**, 6087–6096.

12 X. H. Zhao, S. N. Ma, H. Long, H. Yuan, C. Y. Tang, P. K. Cheng and Y. H. Tsang, *ACS Appl. Mater. Interfaces*, 2018, **10**, 3986–3993.

13 Y. Huang, S. V. Kershaw, Z. Wang, Z. Pei, J. Liu, Y. Huang, H. Li, M. Zhu, A. L. Rogach and C. Zhi, *Small*, 2016, **12**, 3393–3399.

14 Y. Q. Li, W. B. Zhu, X. G. Yu, P. Huang, S. Y. Fu, N. Hu and K. Liao, *ACS Appl. Mater. Interfaces*, 2016, **8**, 33189–33196.

15 Y. Q. Li, P. Huang, W. B. Zhu, S. Y. Fu, N. Hu and K. Liao, *Sci. Rep.*, 2017, **7**, 45013.

16 A. D. Dillon, M. J. Ghidiu, A. L. Krick, J. Griggs, S. J. May, Y. Gogotsi, M. W. Barsoum and A. T. Fafarman, *Adv. Funct. Mater.*, 2016, **26**, 4162–4168.

17 Z. Zhou, J. Liu, X. Zhang, D. Tian, Z. Zhan and C. Lu, *Adv. Mater. Interfaces*, 2019, **6**, 1802040.

18 X. Jiang, W. Li, T. Hai, R. Yue, Z. Chen, C. Lao, Y. Ge, G. Xie, Q. Wen and H. Zhang, *npj 2D Mater. Appl.*, 2019, **3**, 34.

19 S. J. Wang, D. S. Li and L. Jiang, *Adv. Mater. Interfaces*, 2019, **6**, 1900961.

20 Z. Lin, J. Liu, W. Peng, Y. Zhu, Y. Zhao, K. Jiang, M. Peng and Y. Tan, *ACS Nano*, 2020, **14**, 2109–2117.

21 S. Luo, S. Patole, S. Anwer, B. Li, T. Delclos, O. Gogotsi, V. Zahorodna, V. Balitskyi and K. Liao, *Nanotechnology*, 2020, **31**, 395704.

22 Z. Ling, C. E. Ren, M.-Q. Zhao, J. Yang, J. M. Giammarco, J. Qiu, M. W. Barsoum and Y. Gogotsi, *Proc. Natl. Acad. Sci.*, 2014, **111**, 16676–16681.

23 K. Zhang, J. Sun, J. Song, C. Gao, Z. Wang, C. Song, Y. Wu and Y. Liu, *ACS Appl. Mater. Interfaces*, 2020, **12**, 45306–45314.

24 Z. Sun, K. Qu, Y. You, Z. Huang, S. Liu, J. Li, Q. Hu and Z. Guo, *J. Mater. Chem. A*, 2021, **9**, 7278–7300.

25 R. Liu, M. Miao, Y. Li, J. Zhang, S. Cao and X. Feng, *ACS Appl. Mater. Interfaces*, 2018, **10**, 44787–44795.

26 C. Cai, W. Zhou and Y. Fu, *Chem. Eng. J.*, 2021, **418**, 129275.

27 Q. Guo, X. Zhang, F. Zhao, Q. Song, G. Su, Y. Tan, Q. Tao, T. Zhou, Y. Yu, Z. Zhou and C. Lu, *ACS Nano*, 2020, **14**, 2788–2797.

28 J. Yan, C. E. Ren, K. Maleski, C. B. Hatter, B. Anasori, P. Urbankowski, A. Sarycheva and Y. Gogotsi, *Adv. Funct. Mater.*, 2017, **27**, 1701264.

29 Y. Zhao, F. Fang, H.-M. Xiao, Q.-P. Feng, L.-Y. Xiong and S.-Y. Fu, *Chem. Eng. J.*, 2015, **270**, 528–534.

30 X. Gu, Y. Wang, C. Lai, J. Qiu, S. Li, Y. Hou, W. Martens, N. Mahmood and S. Zhang, *Nano Res.*, 2014, **8**, 129–139.

31 M. Guan, X. An and H. Liu, *Cellulose*, 2019, **26**, 2613–2624.

32 Q. C. Liu, T. Liu, D. P. Liu, Z. J. Li, X. B. Zhang and Y. Zhang, *Adv. Mater.*, 2016, **28**, 8413.

33 J. Cao, Z. Zhou, Q. Song, K. Chen, G. Su, T. Zhou, Z. Zheng, C. Lu and X. Zhang, *ACS Nano*, 2020, **14**, 7055–7065.

34 U. G. Wegst, H. Bai, E. Saiz, A. P. Tomsia and R. O. Ritchie, *Nat. Mater.*, 2015, **14**, 23–36.

35 X. Yang and E. D. Cranston, *Chem. Mater.*, 2014, **26**, 6016–6025.

36 S. Sharma, A. Chhetry, S. Zhang, H. Yoon, C. Park, H. Kim, M. Sharifuzzaman, X. Hui and J. Y. Park, *ACS Nano*, 2021, **15**, 4380–4393.

37 Y. Y. Wang, X. Q. Wang, Y. Q. Li, P. Huang, B. Yang, N. Hu and S. Y. Fu, *ACS Appl. Mater. Interfaces*, 2020, **13**, 1431–1440.

38 S. K. Khatua, P. K. Sahoo, K. Kumari, M. Srivatsava, D. Sahu and N. Dalai, *Mater. Today: Proc.*, 2021, **47**, 3633–3636.

39 Y. Q. Li, T. Yu, T. Y. Yang, L. X. Zheng and K. Liao, *Adv. Mater.*, 2012, **24**, 3426–3431.

40 T. Ma, Y. Zhao, K. Ruan, X. Liu, J. Zhang, Y. Guo, X. Yang, J. Kong and J. Gu, *ACS Appl. Mater. Interfaces*, 2020, **12**, 1677–1686.

41 G. Chen, T. Chen, K. Hou, W. Ma, M. Tebyetekerwa, Y. Cheng, W. Weng and M. Zhu, *Carbon*, 2018, **127**, 218–227.

42 W.-B. Zhu, Y.-Q. Li, J. Wang, Y.-Y. Wang, P. Huang, N. Hu, K. Liao and S.-Y. Fu, *ACS Appl. Bio Mater.*, 2020, **3**, 8748–8756.

43 L. Ding, Y. Wei, L. Li, T. Zhang, H. Wang, J. Xue, L. X. Ding, S. Wang, J. Caro and Y. Gogotsi, *Nat. Commun.*, 2018, **9**, 155.

44 A. Lipatov, M. Alhabeb, M. R. Lukatskaya, A. Boson, Y. Gogotsi and A. Sinitskii, *Adv. Electron. Mater.*, 2016, **2**, 1600255.

45 J. D. Currey and A. J. Kohn, *J. Mater. Sci.*, 1976, **11**, 1615–1623.

46 Y. Cheng, Y. An, Y. Liu, Q. Wei, W. Han, X. Zhang, P. Zhou, C. Wei and N. Hu, *ACS Appl. Mater. Interfaces*, 2020, **12**, 33246–33255.

47 B. Zhou, Z. Zhang, Y. Li, G. Han, Y. Feng, B. Wang, D. Zhang, J. Ma and C. Liu, *ACS Appl. Mater. Interfaces*, 2020, **12**, 4895–4905.

48 R. Zou, F. Liu, N. Hu, H. Ning, Y. Gong, S. Wang, K. Huang, X. Jiang, C. Xu, S. Fu, Y. Li and C. Yan, *ACS Appl. Mater. Interfaces*, 2020, **12**, 57391–57400.

49 X. Wu, B. Han, H.-B. Zhang, X. Xie, T. Tu, Y. Zhang, Y. Dai, R. Yang and Z.-Z. Yu, *Chem. Eng. J.*, 2020, **381**, 122622.

50 M. Naguib, T. Saito, S. Lai, M. S. Rager, T. Aytug, M. Parans Paranthaman, M.-Q. Zhao and Y. Gogotsi, *RSC Adv.*, 2016, **6**, 72069–72073.

51

W. T. Cao, F. F. Chen, Y. J. Zhu, Y. G. Zhang, Y. Y. Jiang, M. G. Ma and F. Chen, *ACS Nano*, 2018, **12**, 4583–4593.

52 J. Lipton, G. M. Weng, M. Alhabeb, K. Maleski, F. Antonio, J. Kong, Y. Gogotsi and A. D. Taylor, *Nanoscale*, 2019, **11**, 20295–20300.

53 F. Xie, F. Jia, L. Zhuo, Z. Lu, L. Si, J. Huang, M. Zhang and Q. Ma, *Nanoscale*, 2019, **11**, 23382–23391.

54 W. T. Cao, C. Ma, D. S. Mao, J. Zhang, M. G. Ma and F. Chen, *Adv. Funct. Mater.*, 2019, **29**, 1905898.

55 X. Chen, J. Jiang, G. Yang, C. Li and Y. Li, *Nanoscale*, 2020, **12**, 21325–21333.

56 C. Hu, F. Shen, D. Zhu, H. Zhang, J. Xue and X. Han, *Front. Energy Res.*, 2017, **4**, 41.

57 H. Zhu, S. Zhu, Z. Jia, S. Parvinian, Y. Li, O. Vaaland, L. Hu and T. Li, *Proc. Natl. Acad. Sci. U. S. A.*, 2015, **112**, 8971–8976.

58 G.-M. Weng, J. Li, M. Alhabeb, C. Karpovich, H. Wang, J. Lipton, K. Maleski, J. Kong, E. Shaulsky, M. Elimelech, Y. Gogotsi and A. D. Taylor, *Adv. Funct. Mater.*, 2018, **28**, 1803360.

59 J.-Q. Luo, S. Zhao, H.-B. Zhang, Z. Deng, L. Li and Z.-Z. Yu, *Compos. Sci. Technol.*, 2019, **182**, 107754.

60 X. Jiang, Z. Ren, Y. Fu, Y. Liu, R. Zou, G. Ji, H. Ning, Y. Li, J. Wen, H. J. Qi, C. Xu, S. Fu, J. Qiu and N. Hu, *ACS Appl. Mater. Interfaces*, 2019, **11**, 37051–37059.

61 J. Wen, J. Tang, H. Ning, N. Hu, Y. Zhu, Y. Gong, C. Xu, Q. Zhao, X. Jiang, X. Hu, L. Lei, D. Wu and T. Huang, *Adv. Funct. Mater.*, 2021, **31**, 2011176.

62 S. Wang, H. Ning, N. Hu, Y. Liu, F. Liu, R. Zou, K. Huang, X. Wu, S. Weng and Alamusi, *Adv. Mater. Interfaces*, 2020, **7**, 1901507.

63 Z. Han, H. Li, J. Xiao, H. Song, B. Li, S. Cai, Y. Chen, Y. Ma and X. Feng, *ACS Appl. Mater. Interfaces*, 2019, **11**, 33370–33379.

64 T. Yang and J. M. Mativetsky, *ACS Appl. Mater. Interfaces*, 2019, **11**, 26339–26345.

65 K. Huang, H. Ning, N. Hu, F. Liu, X. Wu, S. Wang, Y. Liu, R. Zou, W. Yuan, Alamusi and L. Wu, *Compos. Sci. Technol.*, 2020, **192**, 108105.

66 S. Choi, J. Park, W. Hyun, J. Kim, Y. B. Lee, C. Song, H. J. Hwang, J. H. Kim, T. Hyeon and D. H. Kim, *ACS Nano*, 2015, **9**, 6626–6633.

67 Y. Li, Y. A. Samad, K. Polychronopoulou, S. M. Alhassan and K. Liao, *J. Mater. Chem. A*, 2014, **2**, 7759–7765.

68 C. Badgwell Doherty, S. D. Doherty and T. Rosen, *J. Am. Acad. Dermatol.*, 2010, **62**, 909–927.

69 J. Luo, S. Gao, H. Luo, L. Wang, X. Huang, Z. Guo, X. Lai, L. Lin, R. K. Y. Li and J. Gao, *Chem. Eng. J.*, 2021, **406**, 126898.

70 Z. Xiao, C. Sheng, Y. Xia, X. Yu, C. Liang, H. Huang, Y. Gan, J. Zhang and W. Zhang, *J. Ind. Eng. Chem.*, 2019, **71**, 293–300.

71 D. Wang, D. Li, M. Zhao, Y. Xu and Q. Wei, *Appl. Surf. Sci.*, 2018, **454**, 218–226.

72 X. Zhao, L. Y. Wang, C. Y. Tang, X. J. Zha, Y. Liu, B. H. Su, K. Ke, R. Y. Bao, M. B. Yang and W. Yang, *ACS Nano*, 2020, **14**, 8793–8805.

73 X. Zheng, J. Shen, Q. Hu, W. Nie, Z. Wang, L. Zou and C. Li, *Nanoscale*, 2021, **13**, 1832–1841.

74 Z. Zhao, J. Zhou, H. Xiao, Y. Liu and M. Lu, *Mater. Today Commun.*, 2020, **24**, 101042.

75 Y. Guo, C. Dun, J. Xu, J. Mu, P. Li, L. Gu, C. Hou, C. A. Hewitt, Q. Zhang, Y. Li, D. L. Carroll and H. Wang, *Small*, 2017, **13**, 1702645.

76 M. R. Lukatskaya, O. Mashtalir, C. E. Ren, Y. Dall'Agnese, P. Rozier, P. L. Taberna, M. Naguib, P. Simon, M. W. Barsoum and Y. Gogotsi, *Science*, 2013, **341**, 1502–1505.

77 M. Ghidiu, M. R. Lukatskaya, M.-Q. Zhao, Y. Gogotsi and M. W. Barsoum, *Nature*, 2014, **516**, 78–81.

78 H. Zhang, L. Lin, B. Wu and N. Hu, *J. Power Sources*, 2020, **476**, 228527.

Footnotes

Queries and Answers

Q1

Query: Have all of the author names been spelled and formatted correctly? Names will be indexed and cited as shown on the proof, so these must be correct. No late corrections can be made.

Answer: The name of "You Yong Wang " has been changed to "You-Yong Wang" is corrected. Other author names are correct.

Q2

Query: Is the inserted Graphical Abstract text suitable? If you provide replacement text, please ensure that it is no longer than 250 characters (including spaces).

Answer: Yes, it is.

Q3

Query: The sentence beginning "Moreover, the MXene/BF composite paper" has been altered for clarity. Please check that the meaning is correct.

Answer: The meaning is correct.

Q4

Query: The sentence beginning "More importantly" has been altered for clarity. Please check that the meaning is correct.

Answer: The meaning is correct.

Q5

Query: The caption to Fig. 3 has been altered for clarity. Please check that the meaning is correct.

Answer: The meaning is correct.

Q6

Query: The meaning of the word "alternation" in the sentence beginning "The contact area increases…" is not clear – please provide alternative text.

Answer: The sentence has been corrected.

Q7

Query: The sentence beginning "Notably, the MXene/BF supercapacitor" has been altered for clarity. Please check that the meaning is correct.

Answer: The meaning is correct.

Q8

Query: Have all of the funders of your work been fully and accurately acknowledged?

Answer: All the funders have been fully and accurately acknowledged.

Q9

Query: Ref. 62: Please provide the initial(s) for the 10th author.

Answer: Alamusi is his full name.

Q10

Query: Ref. 65: Please provide the initial(s) for the 10th author.

Answer: Alamusi is his full name.